Annual Appearance of Hydrogen Chloride on Mars and a Striking Similarity With the Water Vapor Vertical Distribution Observed by TGO/NOMAD

S. Aoki, F. Daerden, S. Viscardy, I. R. Thomas, Justin T. Erwin, S. Robert, L. Trompet, L. Neary, G. L. Villanueva, G. Liuzzi, et al.

Annual appearance of hydrogen chloride on Mars and a striking similarity with the water vapor vertical distribution observed by TGO/NOMAD

S. Aoki[1,2,3 ǂ*], F. Daerden[2 ǂ], S. Viscardy[2 ǂ], I. R. Thomas[2], J. T. Erwin[2], S. Robert[2,4], L. Trompet[2], L. Neary[2], G. L. Villanueva[5], G. Liuzzi[5,6], M. M. J. Crismani[5,7], R.T. Clancy[8], J. Whiteway[9], F. Schmidt[10], M. A. Lopez-Valverde[11], B. Ristic[2], M. R. Patel[12,13], G. Bellucci[14], J.-J. Lopez-Moreno[11], K. S. Olsen[15], F. Lefèvre[16], F. Montmessin[16], A. Trokhimovskiy[17], A. A. Fedorova[17], O. Korablev[17], A. C. Vandaele[2]

(ǂ these authors contributed equally to this work)

1. Institute of Space and Astronautical Science (ISAS), Japan Aerospace Exploration Agency (JAXA), 3-1-1 Yoshinodai, Sagamihara, Kanagawa 252-5210, Japan

2. Royal Belgian Institute for Space Aeronomy, 3 Avenue Circulaire, 1180 Brussels, Belgium

3. LPAP, STAR Institute, Université de Liège, Allée du 6 août, 19C, 4000 Liège, Belgium

4. Institute of Condensed Matter and Nanosciences, Université catholique de Louvain, Chemin du Cyclotron 2, 1348 Louvain-la-Neuve, Belgium

5. NASA Goddard Space Flight Center, 8800 Greenbelt Rd., Greenbelt, 20771 MD, USA

6. Department of Physics, College of Arts and Sciences, American University, 20016 Washington DC, USA

7. California State University, San Bernardino, San Bernardino, CA, 92407, USA

8. Space Science Institute, 4750 Walnut Street, Suite 205, Boulder, CO 80301, USA

9. Centre for Research in Earth and Space Science, York University, Toronto, Ontario M3J 1P3, Canada

10. Université Paris-Saclay, CNRS, GEOPS, 91405, Orsay, France

11. Instituto de Astrofisica de Andalucia, Glorieta de la Astronomia, 18008 Granada, Spain

12. School of Physical Sciences, The Open University, Milton Keynes, MK7 6AA, UK

13. Space Science and Technology Department, Science and Technology Facilities Council, Rutherford Appleton Laboratory, Oxfordshire, U.K.

14. Istituto di Astrofisica e Planetologia Spaziali, Via del Fosso del Cavaliere 100, Roma, Italy

15. Department of Physics, University of Oxford, Oxford, UK.

16. Laboratoire Atmosphères, Milieux, Observations Spatiales (LATMOS/CNRS), Paris, France.

17. Space Research Institute (IKI), Moscow, Russia.

* Corresponding author: Shohei Aoki (aoki.shohei@jaxa.jp)

Key Points (< 140 char. for each):

- Increase of HCl during the southern summer is annually repeated. It shows that HCl formation is independent from a global dust storm.
- Vertical distributions of HCl are strikingly similar to water vapor. It suggests that uptake by water ice clouds plays an important role.
- A rapid decrease of HCl at the end of the southern summer suggests the presence of a strong sink in addition to the photochemical loss.

Abstract

Hydrogen chloride (HCl) was recently discovered in the atmosphere of Mars by two spectrometers onboard the ExoMars Trace Gas Orbiter. The reported detection made in Martian Year 34 was transient, present several months after the global dust storm during the southern summer season. Here we present the full dataset of vertically resolved HCl detections obtained by the NOMAD instrument, which covers also Martian year 35. We show that the particular increase of HCl abundances in the southern summer season is annually repeated, and that the formation of HCl is independent from a global dust storm event. We also find that the vertical distribution of HCl is strikingly similar to that of water vapor, which suggests that the uptake by water ice clouds plays an important role. The observed rapid decrease of HCl abundances at the end of the southern summer would require a strong sink independent of photochemical loss.

Plain Language Summary

A new species, hydrogen chloride (HCl), was recently discovered in the atmosphere Mars. Whereas this gas plays a key role in the atmospheric chemistry on Earth and Venus, the chlorine cycle on Mars is not understood. HCl was found just after the global dust storm, so a connection between the storm and appearance of HCl was suggested. This study shows that HCl is detected even in a year without a global dust storm, which demonstrates that the formation of HCl is primary independent from global dust storms. This study also finds that the vertical distributions of HCl and water vapor are strikingly similar in shape. As the vertical profile of water vapor is controlled by the formation of water ice clouds, it suggests that HCl is taken up by water ice clouds. Finally, we observe that HCl is rapidly disappearing at the end of the southern summer on Mars. We demonstrate that this fast destruction cannot be explained by the standard photochemistry, which suggests that another (unknown) process plays a key role.

1. Introduction

Chlorine chemistry plays an important role in the atmosphere of Earth and Venus. On Earth, small amounts of chlorine can have a dramatic impact on stratospheric ozone (e.g. Solomon, 1999). On Venus, chlorine is involved in the main photochemical cycles (e.g. Mahieux et al., 2015; Sandor and Clancy, 2018). In contrast, on Mars, chlorine photochemistry was considered to be negligible because of the low upper limits provided by the previous measurements (Krasnopolsky et al., 1997: Hartogh et al., 2010; Villanueva et al., 2013). However, the first detection of hydrogen chloride (HCl) in the atmosphere of Mars was made by the Atmospheric Chemistry Suite (ACS) and also confirmed by the Nadir and Occultation for Mars Discovery (NOMAD) onboard the ESA-Roskosmos ExoMars Trace Gas Orbiter (TGO) (Korablev et al., 2021). This discovery of HCl is the first detection of any chlorine species in the Martian atmosphere. It demonstrates an active presence of chlorine photochemistry and HCl is expected to be the main reservoir of chlorine species in the atmosphere of Mars (Lefèvre and Krasnopolsky, 2017). Perchlorate salts ClO_4^- (Hecht et al., 2009; Glavin et al., 2013) and chloride-bearing minerals Cl^- (Osterloo et al., 2008, 2010) are known to be widely present at the

Mars surface, thus an interaction between surface and atmosphere may support chlorine photochemistry. Model and laboratory studies investigated the potential role of atmospheric photochemical processes in the formation of perchlorates (e.g. Catling et al., 2010; Smith et al., 2014; Wilson et al., 2016; Wu et al., 2018, and references therein). However, the chlorine cycle on Mars is still not understood. The discovery made by Korablev et al. (2021) hints at the transient nature of HCl: the detections are mainly confined after the global dust storm in the southern summer season. The observed fast temporal variation can be a key to identify the formation and destruction mechanisms of HCl. The discovery was based on the data taken in Martian year (MY) 34. This study presents the results of the extended NOMAD dataset that also includes almost the full MY 35. We investigate the vertical distribution of HCl volume mixing ratios (vmr) and their similarities with simultaneously obtained water vapor and aerosol profiles. An analysis of the Cl isotopic ratio in HCl with the NOMAD data is presented in an accompanying paper (Luizzi et al., 2021).

2. Methods

2.1 Instrument - NOMAD onboard TGO

NOMAD, a spectrometer operating in the spectral ranges between 0.2 and 4.3 μm onboard ExoMars TGO (Vandaele et al., 2018), has 3 spectral channels: a solar occultation channel (SO – Solar Occultation; 2.3–4.3 μm), a second infrared channel capable of nadir, solar occultation, and limb sounding (LNO – Limb Nadir and solar Occultation; 2.3–3.8 μm), and an ultraviolet/visible channel (UVIS – Ultraviolet and Visible Spectrometer, 200–650 nm). The infrared channels (SO and LNO) have relatively high spectral resolution ($\lambda/d\lambda$~10,000–20,000) provided by an echelle grating used in combination with an Acousto Optical Tunable Filter (AOTF) which selects diffraction orders (Neefs et al., 2015). The sampling rate for the solar occultation measurement is 1 second, which provides high vertical sampling (~1 km) with high vertical resolution (~2 km) from near the surface to 200 km altitude. Thanks to the instantaneous change of the observing diffraction orders achieved by the AOTF, the SO channel is able to measure five or six different diffraction orders per second in solar occultation mode. One of the most remarkable capabilities of NOMAD is its high spectral resolution in the infrared range. This supports investigations of: (1) vertical profiles for atmospheric constituents such as carbon dioxide, carbon monoxide, water vapor, and their isotopic ratios (Vandaele et al., 2019; Aoki et al., 2019; Villanueva et al., 2020); and (2) sensitive searches for organic species (such as CH_4, C_2H_4, C_2H_6, H_2CO; Korablev et al., 2019; Knutsen et al. 2021) and other trace gases (such as HCl, HCN, HO_2, H_2S, N_2O, OCS) by solar occultation measurements with the SO channel. In this study, we analyze the solar occultation measurements acquired by the NOMAD SO channel during the period from 22 April 2018 to 18 December 2020 (from a solar longitude (L_s) of 163° in MY 34 to L_s = 333° in MY 35), which covers southern summer periods in MY 34 and 35. For the current study, a total of 732 occultations that include diffraction order 129 (2889–2921 cm^{-1}) or 130 (2920–2943 cm^{-1}) have been processed. These two diffraction orders contain a strong HCl line (see **Figure 1**) and are normally acquired together with diffraction order 134 (3010-3034 cm^{-1}), order 136 (3056-3080 cm^{-1}), or order 145 (3258-3284 cm^{-1}), which include strong water lines in support of direct comparisons between HCl and water vapor vertical profiles.

2.2 Retrieval of HCl and water vapor volume mixing ratio

The reduction and analysis of the NOMAD data is basically conducted with the same methodology as the previous water vapor study (Vandaele et al., 2019; Aoki et al., 2019). The retrievals of HCl and H_2O are performed with the ASIMUT-ALVL radiative transfer and inversion code (Vandaele et al., 2006). H_2O, HDO, CO_2 and HCl molecular absorptions are taken into account in the radiative transfer calculation and the absorptions are calculated using the following spectroscopic database: HITRAN 2016 database (Gordon et al. 2016) for CO_2 and HCl, and the water line list for CO_2-rich atmospheres by Gamache et al. (2016) for H_2O and HDO. The temperature, pressure, and CO_2 volume mixing ratio of the simulated atmosphere is obtained from the Global Environmental Multiscale Mars model (GEM-Mars) (Neary and Daerden, 2018; Daerden et al., 2019) which takes into account the effects of the global dust storm in MY34 (Neary et al., 2020). The HCl and H_2O retrievals are performed using the Optimal Estimation Method (OEM) (Rodgers, 2000) for each spectrum at each tangential altitude independently. The retrieved HCl and H_2O abundances are finally averaged with an interval of 2 km to obtain the vertical profiles. The averages are weighted by their standard errors (weighted average). In addition to the HCl and H_2O abundances, the vertical profiles of aerosols extinction are investigated. The extinction profiles are simply derived from the averaged transmittances (at diffraction order 129 or 130) based on the onion-peeling method (Wilquet et al., 2012). **Figure 1** shows an example of the NOMAD spectra at diffraction order 129 (**Fig. 1a**) and order 130 (**Fig. 1b**). Clear signatures of HCl are identified at 2906.24 cm^{-1} in order 129 and 2925.89 cm^{-1} in order 130. HCl is usually detected in the lower atmosphere (< 20-25 km) but sometimes up to 35-40 km altitude as shown in **Fig 1b**.

3. Results

3.1 Seasonal, spatial, and interannual variations of HCl

Figures 2a-c show the season-latitude maps of the maximum HCl volume mixing ratio below 30 km observed by NOMAD in MY 34 (**Fig. 2a**), MY 35 (**Fig. 2b**), and plotted together (**Fig. 2c**). As shown in Korablev et al. (2021), a few ppbv of transient HCl was detected in the Mars atmosphere. In MY 34, two strong dust storms occurred on Mars – the global dust storm at L_s=190°-250° and the regional dust storm at L_s=320°-340° (e.g., Aoki et al., 2019; Liuzzi et al., 2020). Almost all of the HCl detections were made in the period between the two dust storms (L_s=240°-320°) (**Fig. 2a**). The period of HCl detections also correspond to the southern summer season on Mars. The temporal variation of the HCl detections in MY 35 is similar to that in MY 34: most of the HCl detections are made in the southern summer period (L_s=240°-320°) (**Fig. 2b**). We use the dust climatology of MY 31 as a proxy, as it looks similar to that of MY 35. Since there is no global dust storm in MY35, it is demonstrated that the formation of HCl is independent from a global dust storm event. In both MY 34 and 35, higher abundances of HCl are observed in the southern hemisphere (local summer, L_s=270°), particularly at high latitudes, which corresponds in time and location to the water vapor enhancement caused by the south polar cap sublimation (**Fig. 2c**). Because the observations before L_s~240° were not possible in the southern hemisphere due to dust obscuration, it is unclear whether this represents an increase in HCl, or if high abundances were already present. In contrast, the volume mixing ratio of HCl is below the detection limit (~0.3 ppbv) at the northern hemisphere summer solstice (L_s=90°), even at high latitudes where the column integrated abundances of water vapor are large.

Figure 2d shows the geographical distribution of the maximum HCl volume mixing ratio below 30 km observed by NOMAD in the southern summer period (L_s=240°-320°) of MY 34

and 35. The detections are dispersed over all observed longitudes, such that HCl is not confined to a specific longitude region. Most of the detections are performed at latitudes higher than 45°. This is because higher dust content in the atmosphere at lower latitudes obscures solar occultation viewing. In other words, the non-detection of HCl at low-latitudes means that the abundance of HCl cannot be measured there. There is a clear north-south asymmetry – the maximum volume mixing ratio of HCl is larger in the southern hemisphere than in the northern hemisphere.

3.2 Vertical distribution of hydrogen chloride, water vapor, and aerosols

Figure 3 shows several representative vertical profiles of HCl, water vapor, and aerosol extinction observed during the same occultation. The seasonal variations of the HCl vertical distributions measured in MY 34 and 35 are quite similar. At northern mid-latitudes (50°-60°N) around perihelion (L_s=240°-270°) (**Fig. 3a)**, water vapor volume mixing ratios increased towards the higher altitudes with a maximum around 30 km. This decrease below 30 km reflects water vapor loss at lower altitudes due to the condensation over the seasonal polar cap (e.g. Daerden et al., 2019). In MY 34, because of increased upper level transport associated with the global dust storm, water is also enhanced at higher altitudes (Aoki et al., 2019; Neary et al., 2020; Fedorova et al., 2020). HCl also shows a decrease towards lower altitudes. At the southern mid-to-high latitudes (50°-70°S) during the same period (**Fig. 3b**), water vapor volume mixing ratios are constant throughout the atmosphere and HCl follows this same uniform distribution.

This constant mixing continues after perihelion (L_s=270°-300°), although in MY 35, water and HCl vmr start to decrease between 20-30 km (**Fig. 3c**). Note that in this seasonal range at L_s=270°-300°, we observe larger water vapor mixing ratios (because of the sublimation of the south polar cap) as well as the largest observed HCl vmr (4 ppbv) both in MY 34 and 35. Moreover, HCl is detected at the highest altitudes (35-40 km). Water vapor is still abundant in the later period (L_s=300°-330°) but rapidly drops above the hygropause, which is located around 15-20 km (**Fig. 3d**). Interestingly, HCl also dramatically drops at the same altitudes. Finally, in the northern hemisphere during the summer solstice (L_s=90°-120°) (**Fig. 3e**), HCl is not detected anymore while a large amount of water vapor is observed at lower altitudes (below 10 km) because of the sublimation of the northern polar cap. This is a low-dust season, and the upper limit of HCl below 10 km is ~ 0.3 ppbv, which is well below the abundances detected in the southern summer season.

Such a temporal variation of the HCl vertical profiles observed by NOMAD is consistent with the simultaneous measurements by ACS reported earlier (Korablev et al., 2021). In this study, we emphasize that the vertical structures of HCl and water vapor are strikingly similar. **Fig. 4a-b** shows the HCl vmr against scaled water vapor vmr for all the HCl detections below 25 km. The water vapor mixing ratios in this figure were scaled for each profile by the ratio of the partial column densities of HCl and water vapor below 25 km (see Supporting Information, SI, Section S1, for more details). This scaling process comes down to shifting the upper and lower x-axes in **Fig. 3** such that the lower part of the HCl and H_2O profiles are overlapping, and so allows us to evaluate the similarity in the shapes of the vertical distributions. The partial column densities were calculated using collocated GEM-Mars temperature and pressure profiles (Daerden et al., 2019; Neary et al., 2020) for the altitudes where HCl was detected. It was preferred to work with partial column densities rather than the ratio of the vmr at one specific

altitude level, because there is no unique altitude level at which HCl was detected in all the profiles.

Fig. 4a-b demonstrates a strong similarity of the shapes of HCl and water vapor vertical structures in the perihelion season. The water vapor profile is shaped by the formation of clouds and their subsequent sedimentation over the course of one or many consecutive sols, counteracting the ascend of water vapor with the normal circulation (Neary et al., 2020). This causes a decrease of the water vapor vmr at the "hygropause" level (e.g., Daerden et al., 2019, their Fig. 13). In polar winter conditions, the water vapor profile is also decreasing towards the surface due to strong surface deposition. We see both types of profiles in Fig. 3. The similarity of the HCl profiles to those of water vapor suggests that HCl is depositing with water vapor, both at the hygropause and at the surface in polar winter. Laboratory work for temperatures (194-228 K) and pressures (133 Pa) representative of Mars (Kippenberger et al., 2019), and for similar HCl partial pressures as found here, demonstrated an extensive, continuous uptake of HCl in water ice during growth of ice particles. This seems to indicate that HCl, once introduced in the atmosphere, tracks with water vapor. However, this behavior does not address the ultimate source or loss processes for Mars atmospheric HCl, as will be discussed below. When the ratio HCl/H_2O is plotted for all the profiles combined, it is not decreasing over time and altitude (**Fig. 4c-d**). This could imply that the uptake of HCl on water ice clouds is not a permanent sink and that HCl is released again when water ice sublimates. However, it can also mean that new chlorine-bearing species are formed at the water ice cloud particles, that can become a new source of HCl (see Discussion for more details).

4. Discussion

4.1 Source of HCl

The first detections of HCl were obtained mainly just after the MY 34 global dust storm. Therefore, Korablev et al. (2021) proposed that dust – including chloride-bearing materials – lifted to high altitudes could release chlorine into the atmosphere by UV irradiation. This would ultimately lead to the formation of HCl through the fast reaction of chlorine with hydroperoxyl that results from photolysis of water vapor also lifted to high altitudes (Wilson et al., 2016; Lefèvre and Krasnopolsky, 2017):

$$Cl + HO_2 \rightarrow HCl + O_2 \qquad (1)$$

However, the repeated detections of equivalent HCl abundances in the same season in MY 35 clearly indicates that a global dust storm is not required, the annually enhanced dust abundances in the perihelion season appearing to be sufficient to produce HCl.

The strong enhancement of HCl at the southern high latitudes in the southern summer season suggests that the main source of atmospheric chlorine could be there. We note that further measurement are needed to confirm the source as a large part of the NOMAD observations at low- and mid-latitudes could not detect HCl because of strong dust presence. Nevertheless, if the source is the southern high latitudes, the produced HCl can be transported to the northern hemisphere by the global circulation. Theoretical studies show that the time scale of the global mixing from 60°S latitude to north polar latitudes can be as low as 20 sols or less in this season

(Waugh et al., 2019, their Fig. 1d). This is fast enough to explain the observed latitudinal distribution of HCl.

The combination of enhanced dust and water abundances seems to be the key ingredient for the production of HCl. This may explain why there is no HCl detected in the northern summer season, which, despite the presence of large amounts of water vapor, is relatively dust-free. HCl may still be there, but below the detection limit. Dust optical maps from Montabone et al. (2015, 2020) show a ratio of dust optical depths between perihelion and aphelion of ~5 (even in a low dust year), which could be sufficient to either preclude the formation of HCl in northern summer, or to keep it below detectability. However, detection limits reported in Korablev et al. (2021) (0.1-0.2 ppbv) and here (0.3 ppbv) are much lower than simply scaling the observed HCl abundances by a factor of 5. It is possible that a certain threshold of dust abundance is required for the formation of HCl. Another possibility is that the HCl is released from the southern polar cap together with water vapor. But then the question remains why the same process is not occurring at the northern summer cap. If chlorine species are stored in the seasonal caps and released with water vapor during local spring and summer to form HCl, HCl should be strongly present during northern summer, which is not the case.

4.2 Sink of HCl

Another important issue arising from the reported observations regards the relatively rapid decay of atmospheric HCl abundances, requiring a strong HCl loss rate (Korablev et al., 2021 and Fig. 2 of this article). Indeed, the photochemical lifetime of HCl in the low atmosphere of Mars is estimated to be relatively long (see SI, Section S2). It can vary between >90 sols to >1000 sols below 15 km at the southern and northern mid-latitudes during the northern hemisphere winter solstice (see Fig. S2). On the other hand, the production of HCl through the reaction between Cl and HO_2 is much faster (typically on timescales <10 minutes in the lower atmosphere; see Fig. S2). As a result, HCl is expected to be the primary Cl reservoir species in the Martian atmosphere. In this context, the sudden loss of HCl which is observed around L_s=320° (**Fig. 2**) cannot be explained by gas-phase photochemistry alone. A sink process, in addition to photochemical loss, has to be invoked. Korablev et al. (2021) suggested that HCl could be removed from the atmosphere by uptake in growing water ice clouds particles and/or surface ice (Kippenberger et al., 2019). The striking similarity between HCl and water vapor vertical profiles shown in this study suggests that the vertical distribution of HCl is controlled by water ice clouds. However, the sublimation of those ice particles would be accompanied by the release of chlorine and thus the formation of atmospheric HCl, and thus it looks problematic to explain the permanent removal of HCl from the atmosphere by the uptake of HCl (reversible or irreversible) by water ice clouds.

Another possibility to remove HCl may be heterogeneous reactions on water ice cloud particles. This process is well known on Earth, where such reactions play a role in the formation of the polar ozone hole: $ClONO_2 + HCl \rightarrow Cl_2 + HNO_3$, $N_2O_5 + HCl \rightarrow ClNO_2 + HNO_3$, $HOCl + HCl \rightarrow Cl_2 + H_2O$ (Solomon, 1999). However, even if those reactions could take place efficiently on Mars, the produced chlorinated compounds would be readily converted to Cl radicals by photolysis (on timescales of a few tens of minutes), and subsequently create HCl by Reaction (1). Chlorine can also be removed by the formation of perchlorates (ClO_4^-). The uptake of ClO on ice particles was experimentally observed to lead to the release of chlorine dioxide (OClO) upon ice evaporation (McKeachie et al., 2004). Although the enhanced concentrations of

OClO could favor the production of $HClO_4$ (Catling et al., 2010; Wilson et al., 2016) and the permanent removal of chlorine from the gas phase, this process should be much too slow to explain the rapid loss of HCl.

It remains difficult to explain the disappearance of HCl after L_s=320°. Interestingly, the time of this sudden HCl loss corresponds to the onset of the regional storm (**Fig. 2)** that is annually repeated and recognized as "c" dust storm. This raises the possibility that this dust storm acts as the sink for HCl. In this respect, note that mineral dust was found to be the seat of HCl removal in the Earth's atmosphere (Sullivan et al., 2007). However, these arguments require robust dust-HCl interactions that are not yet established by laboratory studies, and so need to be addressed in the future.

5. Conclusions

In this paper, we present the full dataset of vertically resolved HCl detections derived from the TGO/NOMAD measurements taken between April 2018 and December 2020, which covers southern summer periods in MY 34 and MY 35. The main results are as follows:

1. We find enhancement of HCl at the southern summer period (L_s=240-320°) both in MY 34 and MY 35. It suggests that the global dust storm (which occurred only in MY 34) is not necessary for the formation of HCl.
2. Both in MY 34 and MY 35, a larger abundance of HCl is observed at the southern high latitudes where water vapor sublimates from the southern polar cap.
3. We find that the vertical distributions of HCl and water vapor are strikingly similar in shape. It suggests that once HCl is introduced in the atmosphere, it follows water vapor including uptake in water ice clouds.
4. We show that the lifetime of HCl in the Mars atmosphere is too long to explain the observed rapid loss of HCl in the Mars atmosphere around Ls=320°, which thus requires a strong sink of HCl independent from the photochemical loss.

Acknowledgments, Samples, and Data

ExoMars is a space mission of the European Space Agency and Roscosmos. The NOMAD experiment is led by the Royal Belgian Institute for Space Aeronomy (IASB‐BIRA), assisted by Co‐PI teams from Spain (IAA‐CSIC), Italy (INAF‐IAPS), and the United Kingdom (Open University). This project acknowledges funding by the Belgian Science Policy Office, with the financial and contractual coordination by the European Space Agency Prodex Office (PEA 4000103401 and 4000121493), by the Spanish MICINN through its Plan Nacional and by European funds under grants PGC2018‐101836‐B‐I00 and ESP2017‐87143‐R (MINECO/FEDER), as well as by UK Space Agency through grants ST/V002295/1, ST/V005332/1 ST/S00145X/1 ST/S00145X/1 and ST/T002069/1, and Italian Space Agency through grant 2018‐2‐HH.0. This work was supported by NASA's Mars Program Office under WBS 604796, "Participation in the TGO/NOMAD Investigation of Trace Gases on Mars". The IAA/CSIC team acknowledges financial support from the State Agency for Research of the Spanish MCIU through the "Center of Excellence Severo Ochoa" award for the Instituto de Astrofísica de Andalucía (SEV‐2017‐0709). This work was supported by the Belgian Fonds de la Recherche Scientifique‐FNRS under grant numbers 30442502 (ET_HOME) and T.0171.16

(CRAMIC) and Belgian Science Policy Office BrainBe SCOOP and MICROBE Projects. S. A. is "Chargé de Recherches" at the F.R.S.-FNRS. U.S. investigators were supported by the National Aeronautics and Space Administration. We acknowledge support from the Institut National des Sciences de l'Univers" (INSU), the "Centre National de la Recherche Scientifique" (CNRS) and "Centre National d'Etudes Spatiales" (CNES) through the "Programme National de Planetologie".

The NOMAD data used in this study are available from ESA's Planetary Science Archive at https://archives.esac.esa.int/psa/#!Table%20View/NOMAD=instrument.

References

Aoki, S., A. C. Vandaele, F. Daerden, G. L. Villanueva, G. Liuzzi, I. R. Thomas, J. T. Erwin, L. Trompet, S. Robert, L. Neary, S. Viscardy, R. T. Clancy, M. D. Smith, M. A. Lopez-Valverde, B. Hill, B. Ristic, M. R. Patel, G. Bellucci, J.-J. Lopez-Moreno, and the NOMAD team (2019), Water vapor vertical profiles on Mars in dust storms observed by TGO/NOMAD. J. Geophys. Res.: Planets, 124, 3482-3497, doi:10.1029/2019JE006109.

Catling, D. C., Claire, M. W., Zahnle, K. J., Quinn, R. C., Clark, B. C., Hecht, M. H., and Kounaves, S. (2010), Atmospheric origins of perchlorate on Mars and in the Atacama, J. Geophys. Res. 115, E00E11, doi:10.1029/2009JE003425.

Daerden, F., Neary, L., Viscardy, S., Garcia Munoz, A., Clancy, R. T., Smith, M. D., T. Encrenaz, and A. Fedorova (2019), Mars atmospheric chemistry simulations with the GEM-Mars general circulation model. Icarus, 326, 197–224, doi:10.1016/j.icarus.2019.02.030.

Fedorova, A. A., et al. (2020), Stormy water on Mars: The distribution and saturation of atmospheric water during the dusty season. Science, Vol. 367, Issue 6475, pp. 297-300, doi: 10.1126/science.aay9522.

Gamache, R. R., M. Farese, and C. L. Renaud (2016), A spectral line list for water isotopologues in the 1100-4100 cm^{-1} region for application to CO_2-rich planetary atmospheres, Journal of Molecular Spectroscopy, 326, 144–150, doi:10.1016/j.jms.2015.09.001.

George, I. J. and J. P. D. Abbatt (2010), Heterogeneous oxidation of atmospheric aerosol particles by gas-phase radicals, Nature Chemistry, 2, 713–722, doi:10.1038/nchem.806.

Glavin, D. P. et al. (2013), Evidence for perchlorates and the origin of chlorinated hydrocarbons detected by SAM at the Rocknest aeolian deposit in Gale Crater, J. Geophys. Res., 118, 1955–1973, doi:10.1002/jgre.20144.

Gordon, I. E., L. S. Rothman, C. Hill, R. V. Kochanov, Y. Tan, P. F. Bernath, M. Birk, V. Boudon, A. Campargue, K. V. Chance, B. J. Drouin, J.-M. Flaud, R. R. Gamache, J. T. Hodges, D. Jacquemart, V. I. Perevalov, A. Perrin, K. P. Shine, M.-A. H. Smith, J. Tennyson, G. C. Toon, H. Tran, V. G. Tyuterev, A. Barbe, A. G. Császár, V. M. Devi, T. Furtenbacher, J. J. Harrison, J.-M. Hartmann, A. Jolly, T. J. Johnson, T. Karman, I. Kleiner, A. A. Kyuberis, J. Loos, O. M. Lyulin, S. T. Massie, S. N. Mikhailenko, N. Moazzen-Ahmadi, H. S. P. Müller, O. V. Naumenko, A. V. Nikitin, O. L. Polyansky, M. Rey, M. Rotger, S. W. Sharpe, K. Sung, E. Starikova, S. A. Tashkun, J. Vander Auwera, G. Wagner, J. Wilzewski, P. Wcisło, S.Yu, and E. J. Zak (2017), The HITRAN2016 Molecular

Spectroscopic Database, Journal of Quantitative Spectroscopy and Radiative Transfer, 203, 3–69, doi:10.1016/j.jqsrt.2017.06.038.

Hecht, M. H. et al. (2009), Detection of Perchlorate and the Soluble Chemistry of Martian Soil at the Phoenix Lander Site, Science, 325, 64–67, doi: 10.1126/science.1172466.

Hartogh, P, C. Jarchow, E. Lellouch, M. de Val-Borro, M. Rengel, R. Moreno, A. S. Medvedev, H. Sagawa, B. M. Swinyard, T. Cavalié, D. C. Lis, M. I. Blecka, M. Banaszkiewicz, D. Bockelée-Morvan, J. Crovisier, T. Encrenaz, M. Küppers, L.-M. Lara, S. Szutowicz, B. Vandenbussche, F. Bensch, E. A. Bergin, F. Billebaud, N. Biver, G. A. Blake, J. A. D. L. Blommaert, J. Cernicharo, L. Decin, P. Encrenaz, H. Feuchtgruber, T. Fulton, T. de Graauw, E. Jehin, M. Kidger, R. Lorente, D. A. Naylor, G. Portyankina, M. Sánchez-Portal, R. Schieder, S. Sidher, N. Thomas, E. Verdugo, C. Waelkens, N. Whyborn, D. Teyssier, F. Helmich, P. Roelfsema, J. Stutzki, H. G. LeDuc, and J. A. Stern (2010), Herschel/HIFI observations of Mars: First detection of O2 at submillimetre wavelengths and upper limits on HCl and H2O2, A&A, 521, L49, doi:10.1051/0004-6361/201015160.

Kim, Y. S., K. P. Wo, S. Maity, S. K. Atreya, and R. I. Kaiser (2013), Radiation-Induced Formation of Chlorine Oxides and Their Potential Role in the Origin of Martian Perchlorates, J. Am. Chem. Soc., 135, 4910–4913, doi:10.1021/ja3122922.

Kippenberg, M., G. Schuster, J. Lelieveld, and J. N. Crowley (2019), Trapping of HCl and oxidised organic trace gases in growing ice at temperatures relevant to cirrus clouds, ACP 19, 11939–11951, doi:10.5194/acp-19-11939-2019.

Knutsen, E. W., G. L. Villanueva, G. Liuzzi, M. M. J. Crismani, M. J. Mumma, M. D. Smith, A. C. Vandaele, S. Aoki, I. R. Thomas, F. Daerden, S. Viscardy, J. T. Erwin, L. Trompet, L. Neary, B. Ristic, M. A. Lopez-Moreno, M. R. Patel, O. Karatekin, G. Bellucci (2021), Comprehensive investigation of Mars methane and organics with ExoMars/NOMAD, Icarus, in press, doi:10.1016/j.icarus.2020.114266.

Korablev, O., A. C. Vandaele, F. Montmessin, A. A. Fedorova, A. Trokhimovskiy, F. Forget, F. Lefèvre, F. Daerden, I. R. Thomas, L. Trompet, J. T. Erwin, S. Aoki, S. Robert, L. Neary, S. Viscardy, A. V. Grigoriev, N. I. Ignatiev, A. Shakun, A. Patrakeev, D. A. Belyaev, J.-L. Bertaux, K. S. Olsen, L. Baggio, J. Alday, Y. S. Ivanov, B. Ristic, J. Mason, Y. Willame, C. Depiesse, L. Hetey, S. Berkenbosch, R. Clairquin, C. Queirolo, B. Beeckman, E. Neefs, M. R. Patel, G. Bellucci, J.-J. López-Moreno, C. F. Wilson, G. Etiope, L. Zelenyi, H. Svedhem, J. L. Vago and The ACS & NOMAD Team (2019), No detection of methane on Mars from early ExoMars Trace Gas Orbiter observations, Nature, 568, 517–520, doi:10.1038/s41586-019-1096-4.

Korablev et al. (2021), Transient HCl in the atmosphere of Mars, to appear in Science Advances.

Lefèvre, F. & Krasnopolsky, V. (2017), Atmospheric Photochemistry. in The Atmosphere and Climate of Mars (eds. Haberle, R. M., Clancy, R. T., Forget, F., Smith, M. D. & Zurek, R. W.), Cambridge University Press, p. 405–432.

Liuzzi, G., G. L. Villanueva, M. M. J. Crismani, M. D. Smith, M. J. Mumma, F. Daerden, S. Aoki, A. C. Vandaele , R. T. Clancy, J. Erwin, I. Thomas, B. Ristic, J.-J. Lopez‐Moreno, G. Bellucci, and M. R. Patel (2020), Strong variability of Martian water ice clouds during

dust storms revealed from ExoMars Trace Gas Orbiter/NOMAD. J. Geophys. Res.: Planets, 124, doi:10.1029/2019JE006250.

Liuzzi, G., et al., Probing Atmospheric Cl Isotopic Ratio on Mars: Implications for the Planetary Evolution, Submitted to GRL.

Mahieux, A., V. Wilquet, A.C. Vandaele, S. Robert, R. Drummond, S. Chamberlain, A. Grau Ribes and J.L. Bertaux (2015), Hydrogen halides measurements in the Venus mesosphere retrieved from SOIR onboard Venus Express, Planetary and Space Science, 113-114, 264–274, doi:10.1016/j.pss.2014.12.014.

McKeachie, J. R., M. F. Appel, U. Kirchner, R. N. Schindler, and T. Benter (2004), Observation of a Heterogeneous Source of OClO from the Reaction of ClO Radicals on Ice, J. Phys. Chem. B, 108, 16786-16797, doi:10.1021/jp049314p.

Montabone, L., Forget, F., Millour, E., Wilson, R. J., Lewis, S. R., Cantor, B., Wolff, M. J. (2015), Eight-year climatology of dust optical depth on Mars. Icarus, 251, 65–95. doi:10.1016/j.icarus.2014.12.034.

Montabone, L., A. Spiga, D.M. Kass, A. Kleinböhl, F. Forget, and E. Millour (2020), Martian Year 34 Column Dust Climatology from Mars Climate Sounder Observations: Reconstructed Maps and Model Simulations. J. Geophys. Res. - Planets, doi:10.1029/2019JE006111.

Neary L. and F. Daerden (2018), The GEM-Mars general circulation model for Mars: Description and evaluation, Icarus, 300, 458–476, doi:10.1016/j.icarus.2017.09.028.

Neary L., F. Daerden, S. Aoki, J. Whiteway, R. T. Clancy, M. Smith, S. Viscardy, J. T. Erwin, I. R. Thomas, G. Villanueva, G. Liuzzi, M. Crismani, M. Wolff, S. R. Lewis, J. A. Holmes, M. R. Patel, M. Giuranna, C. Depiesse, A. Piccialli, S. Robert, L. Trompet, Y. Willame, B. Ristic, and A. C. Vandaele (2020), Explanation for the increase in high altitude water on Mars observed by NOMAD during the 2018 global dust storm, Geophys. Res. Lett., 47, e2019GL084354, doi:10.1029/2019GL084354.

Neefs, E., A. C. Vandaele, R. Drummond, I. Thomas, S. Berkenbosch, R. Clairquin, S. Delanoye, B. Ristic, J. Maes, S. Bonnewijn, G. Pieck, E. Equeter, C. Depiesse, F. Daerden, E. Van Ransbeeck, D. Nevejans, J. Rodriguez, J.-J. Lopez-Moreno, R. Sanz, R. Morales, G.P. Candini, C. Pastor, B. Aparicio del Moral, J.M. Jeronimo, J. Gomez, I. Perez, F. Navarro, J. Cubas, G. Alonso, A. Gomez, T. Thibert, M. R. Patel, G. Belucci, L. De Vos, S. Lesschaeve, N. Van Vooren, W. Moelans, L. Aballea, S. Glorieux, A. Baeke, D. Kendall, J. De Neef, A. Soenen, P.Y. Puech, J. Ward, J.F. Jamoye, D. Diez, A. Vicario, and M. Jankowski (2015), NOMAD spectrometer on the ExoMars trace gas orbiter mission: part 1 – design, manufacturing and testing of the infrared channels, Applied Optics, 54 (28), 8494–8520, doi:10.1364/AO.54.008494.

Rodgers, C. D. (2000), Inverse Methods for Atmospheric Sounding - Theory and Practice, Inverse Methods for Atmospheric Sounding - Theory and Practice. Series: Series on Atmospheric Oceanic and Planetary Physics, ISBN: 9789812813718. World Scientific Publishing Co. Pte. Ltd., Edited by Clive D. Rodgers, vol. 2, doi:10.1142/9789812813718.

Sandor B. J. and R. T. Clancy (2018), First measurements of ClO in the Venus atmosphere – Altitude dependence and temporal variation, Icarus, 313, 15–24, doi:10.1016/j.icarus.2018.04.022.

Simonaitis, R. and Heicklen, J. (1975), Perchloric acid: a possible sink for stratospheric chlorine, Planet. Space Sci., 23, 1567–1569, doi:10.1016/0032-0633(75)90010-0.

Smith, M.D. (2002), The Annual Cycle of Water Vapor on Mars as Observed by the Thermal Emission Spectrometer. J. Geophys. Res., 107, doi:10.1029/2001JE001522.

Smith, M.D. (2006), TES Atmospheric Temperature, Aerosol, Optical Depth, and Water Vapor Observations 1999-2004. Second workshop on Mars atmospheric modeling and observations. Granada, Spain, 2006.

Smith, M. L., M. W. Claire, D. C. Catling, and K. J. Zahnle (2014), The formation of sulfate, nitrate and perchlorate salts in the martian atmosphere, Icarus, 231, 51–64, doi:10.1016/j.icarus.2013.11.031.

Solomon, S. (1999), Stratospheric ozone depletion: A review of concepts and history, Rev. Geophys., 37, 275–316, doi:10.1029/1999RG900008.

Sullivan, R. C., S. A. Guazzotti, D. A. Sodeman, Y. Tang, G. R. Carmichael, K. A. Prather (2007), Mineral dust is a sink for chlorine in the marine boundary layer, Atmospheric Environment, 41, 7166–7179, doi:10.1016/j.atmosenv.2007.05.047.

Tabazadeh, A., and R. P. Turco (1993), Stratospheric Chlorine Injection by Volcanic Eruptions: HCI Scavenging and Implications for Ozone, Science, 260, 5111, 1082–1086, doi:10.1126/science.260.5111.1082.

Vandaele, A. C., M. Kruglanski, and M. De Maziere (2006), Simulation and retrieval of atmospheric spectra using ASIMUT, paper presented at Atmospheric Science Conference, Eur. Space Agency, Frascati, Italy.

Vandaele, A. C., J.-J. Lopez-Moreno, M.R. Patel, G. Bellucci, M. Allen, G. Alonso-Rodrigo, F. Altieri, S. Aoki, D. Bolsée, T. Clancy, E. Cloutis, F. Daerden, C. Depiesse, R. Drummond, A. Fedorova, V. Formisano, B. Funke, A. Geminale, J.-C. Gérard, M. Giuranna, N. Ignatiev, J. Kaminski, O. Karatekin, Y. Kasaba, M. Leese, F. Lefèvre, S. Lewis, M. López-Puertas, M. López-Valverde, A. Mahieux, J. Mason, J. McConnell, M. Mumma, L. Neary, E. Neefs, E. Renotte, B. Ristic, S. Robert, J. Rodriguez-Gomez, G. Sindoni, M. Smith, A. Stiepen, I. R. Thomas, A. Trokhimovsky, J. Vander Auwera, G. Villanueva, S. Viscardy, J. Whiteway, Y. Willame, V. Wilquet, M. Wolff, and the NOMAD Team (2018), NOMAD, an integrated suite of three spectrometers for the ExoMars Trace Gas mission: technical description, science objectives and expected performance, Space Science Reviews, 214, 5, article id. 80, 47 pp, doi:10.1007/s11214-018-0517-2.

Vandaele, A. C., O. Korablev, F. Daerden, S. Aoki, I. R. Thomas, F. Altieri, M. López-Valverde, G. L. Villanueva, G. Liuzzi, M. D. Smith, J. T. Erwin, L. Trompet, A. A. Fedorova, F. Montmessin, A. Trokhimovskiy, D. A. Belyaev, N. I. Ignatiev, M. Luginin, K. S. Olsen, L. Baggio, J. Alday, J.-L. Bertaux, D. Betsis, D. Bolsée, R. T. Clancy, E. Cloutis, C. Depiesse, B. Funke, M. Garcia-Comas, J. -C. Gérard, M. Giuranna, F. Gonzalez-Galindo, A. V. Grigoriev, Y. S. Ivanov, J. Kaminski, O. Karatekin, F. Lefèvre, S. Lewis, M. López-

Puertas, A. Mahieux, I. Maslov, J. Mason, M. J. Mumma, L. Neary, E. Neefs, A. Patrakeev, D. Patsaev, B. Ristic, S. Robert, F. Schmidt, A. Shakun, N. A. Teanby, S. Viscardy, Y. Willame, J. Whiteway, V. Wilquet, M. J. Wolff, G. Bellucci, M. R. Patel, J.-J. López-Moreno, F. Forget, C. F. Wilson, H. Svedhem, J. L. Vago, D. Rodionov, NOMAD Science Team, and ACS Science Team (2019), Martian dust storm impact on atmospheric H_2O and D/H observed by ExoMars Trace Gas Orbiter, Nature, 568, 7753, 521–525, doi:10.1038/s41586-019-1097-3.

Villanueva, G.L., M.J. Mumma, R.E. Novak, Y. L. Radeva, H.U. Käufl, A. Smette, A. Tokunaga, A. Khayat, T. Encrenaz, P. Hartogh (2013), A sensitive search for organics (CH_4, CH_3OH, H_2CO, C_2H_6, C_2H_2, C_2H_4), hydroperoxyl (HO_2), nitrogen compounds (N_2O, NH_3, HCN) and chlorine species (HCl, CH_3Cl) on Mars using ground-based high-resolution infrared spectroscopy, Icarus 223, 11–27, doi:10.1016/j.icarus.2012.11.013.

Villanueva, G., L. et al. (2020), Water heavily fractionated with altitude on Mars as revealed by ExoMars/NOMAD, Science Advances, in press.

Waugh, D. W., A. D. Toigo, R. I. Kaiser, and P. R. Mahaffy (2019), Age of martian air: Time scales for martian atmospheric transport, Icarus, 317, 148–157 (2019), doi:10.1016/j.icarus.2018.08.002.

Wilson, E. H., Atreya, S. K., Kaiser, R. I., and Mahaffy, P. R. (2016), Perchlorate formation on Mars through surface radiolysis-initiated atmospheric chemistry: A potential mechanism, J. Geophys. Res. - Planets, 121, 1472–1482 (2016), doi:10.1002/2016JE005078.

Wilquet, V., R. Drummond, A. Mahieux, S. Robert, A.C. Vandaele, and J.-L. Bertaux (2012), Optical extinction due to aerosols in the upper haze of Venus: Four years of SOIR/VEX observations from 2006 to 2010, Icarus, 217, 875–881, doi:10.1016/j.icarus.2011.11.002.

Wu, Z., A. Wang, W. M. Farrell, Y. Yan, K. Wang, J. Houghtonb, A. W. Jacksond, (2018), Forming perchlorates on Mars through plasma chemistry during dust events, Earth and Planetary Science Letters, 504, 94–105, doi:10.1016/j.epsl.2018.08.040.

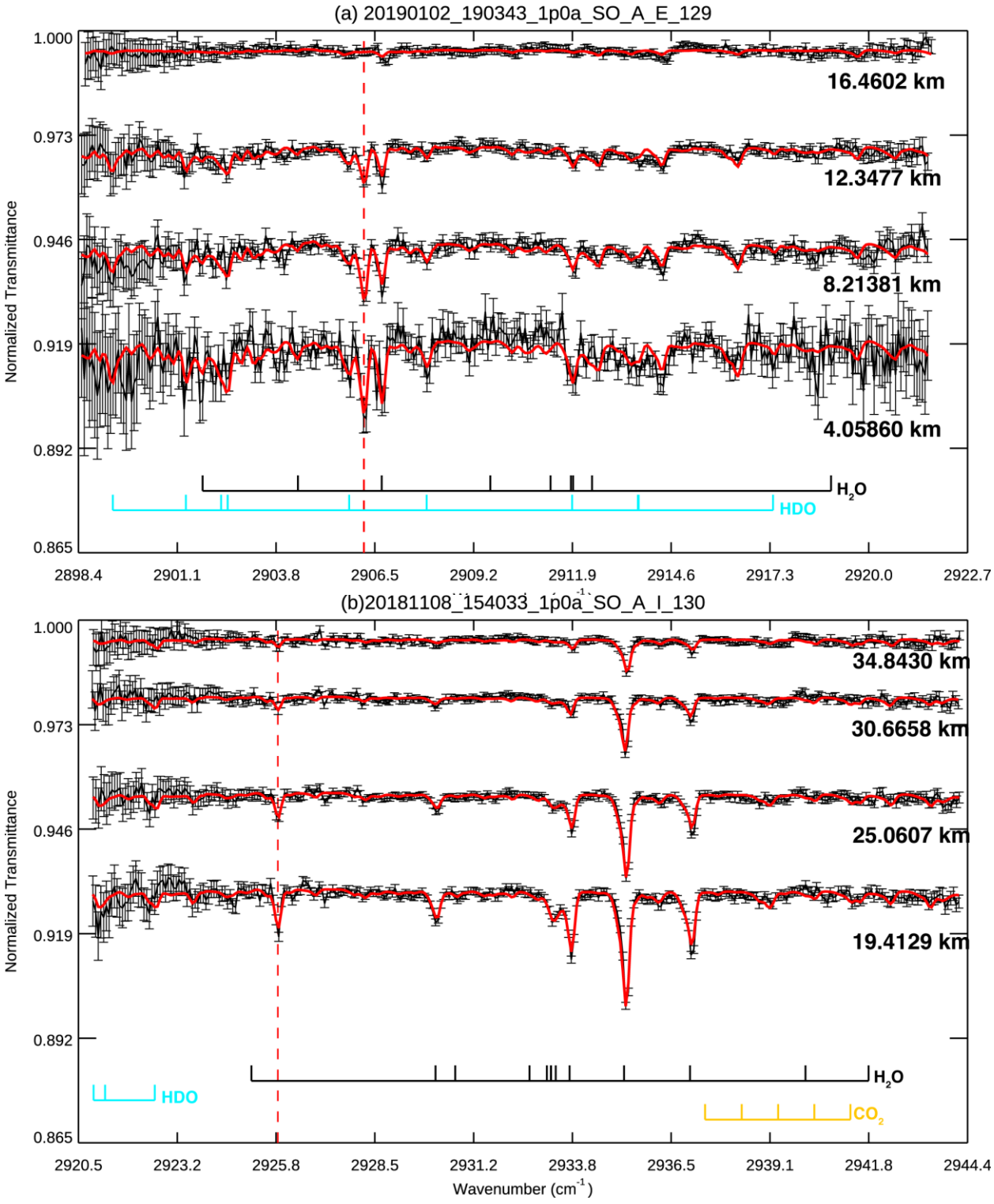

Figure 1. Examples of the NOMAD-SO spectra with signatures of HCl: (a) measurements in the diffraction order 129 performed on 2nd January 2019 (L_s=317.4°, Latitude=72°S, Longitude=46°W); (b) measurements in the diffraction order 130 performed on 8th November 2018 (L_s=284.5°, Latitude=63°S, Longitude=149°E). The best-fit synthetic spectra are shown by

the red curves. The vertical dashed lines in red represent the position of the HCl lines. The other spectral signatures are absorptions due to water vapor and CO_2. The bottom markers show the position of the strong H_2O ($S > 1 \times 10^{-24}$ cm, black), HDO ($S > 1 \times 10^{-24}$ cm, light blue), and CO_2 ($S > 1 \times 10^{-28}$ cm, orange) lines in the main diffraction order.

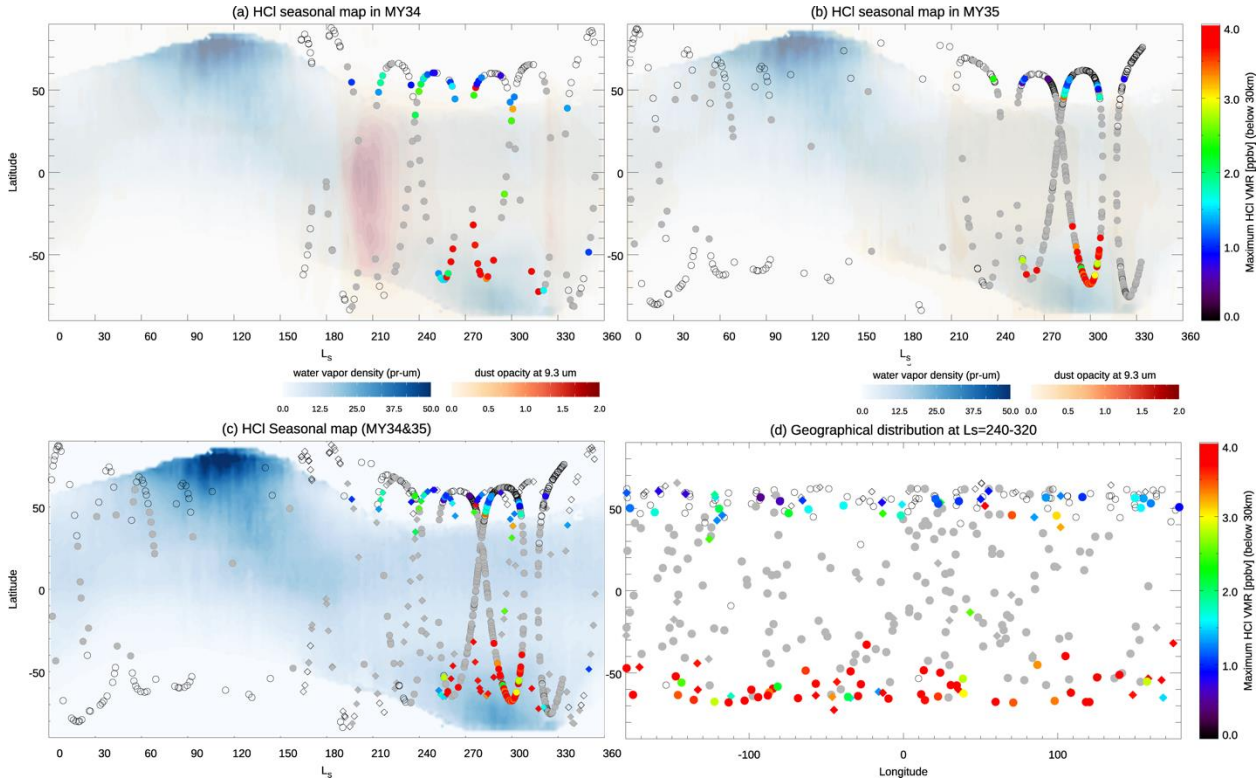

Figure 2. (a-c) Solar longitude - Latitude map of the maximum HCl mixing ratio (ppbv) below 30 km in (a) MY 34, (b) MY 35, and (c) MY34-35 plotted together. Only 3-σ detections are shown here. The gray points show observations corresponding to dust top altitude greater than 25 km, for which it is generally difficult to perform robust retrievals. The background color maps show the column-integrated water vapor density (pr-μm) obtained by MGS/TES for Mars year 26 (Smith, 2002; 2006) and the column-integrated dust opacity at 9.3 μm normalized for 610 Pa for MY 31 (b) and MY 34 (a) (Montabone et al., 2020). (d) Geographical distribution of HCl below 30 km in the seasonal range between L_s=240° and 320°.

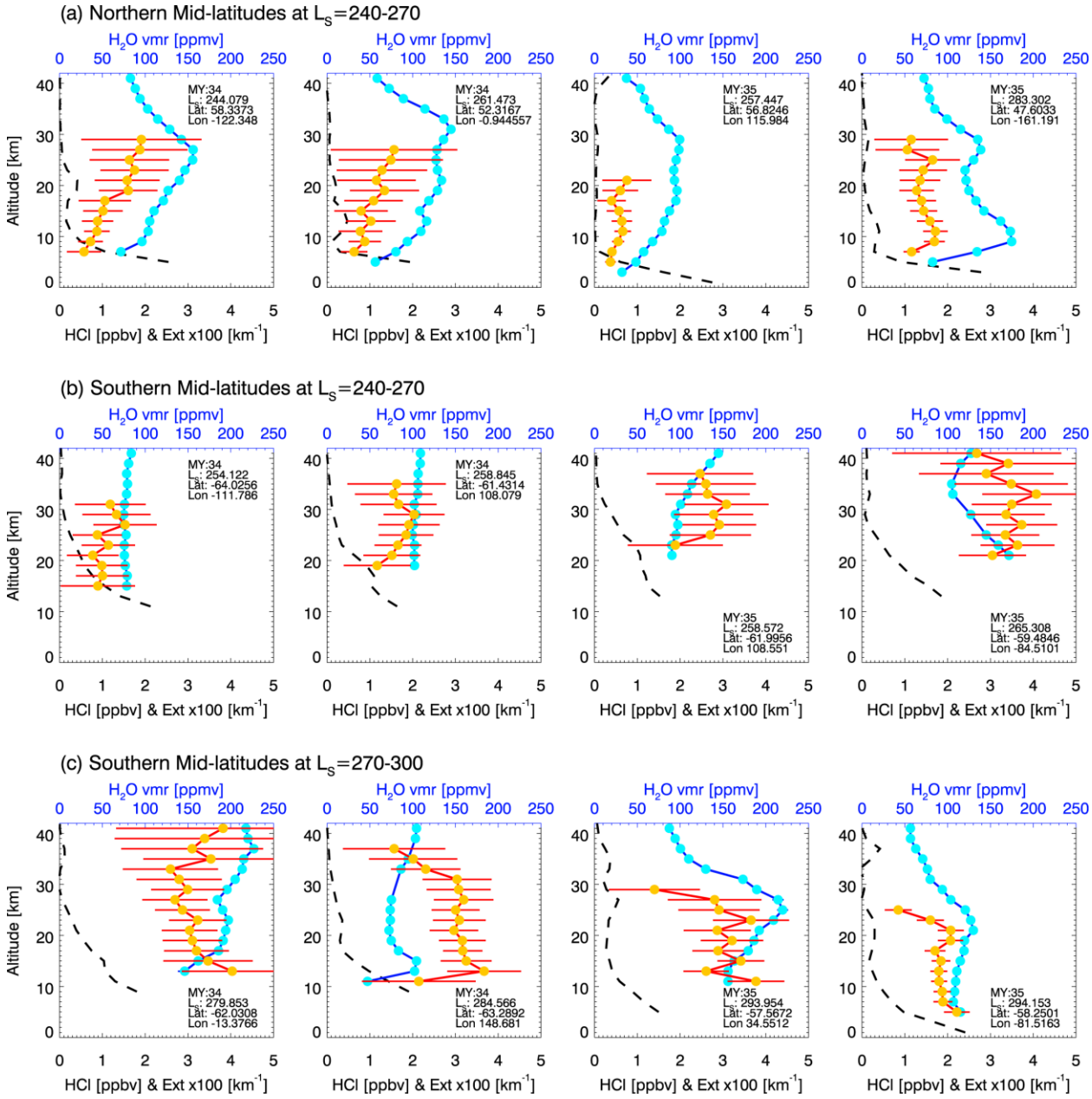

Figure 3. Representative vertical profiles of HCl, water vapor, and aerosols extinction at (a) the northern mid-latitudes (50°-60°N) at L_S=240°-270°; (b) the southern high-latitudes (60°-70°S) during the perihelion (L_S=240°-270°); (c) the southern mid-latitudes (30°S and 60°S) at L_S=270°-300°); (d) the southern high-latitudes (60°S-70°S) at L_S=300°-330°; and (e) the northern mid-latitudes (50°-60°N) at L_S=90°-120°. The red-orange, blue-light blue, and dashed black curves show HCl volume mixing ratio (0-5 ppbv), water vapor mixing ratio (0-250 ppmv), and extinction coefficient (0.00-0.05 km^{-1}) respectively. The error bars represent 3-σ uncertainty.

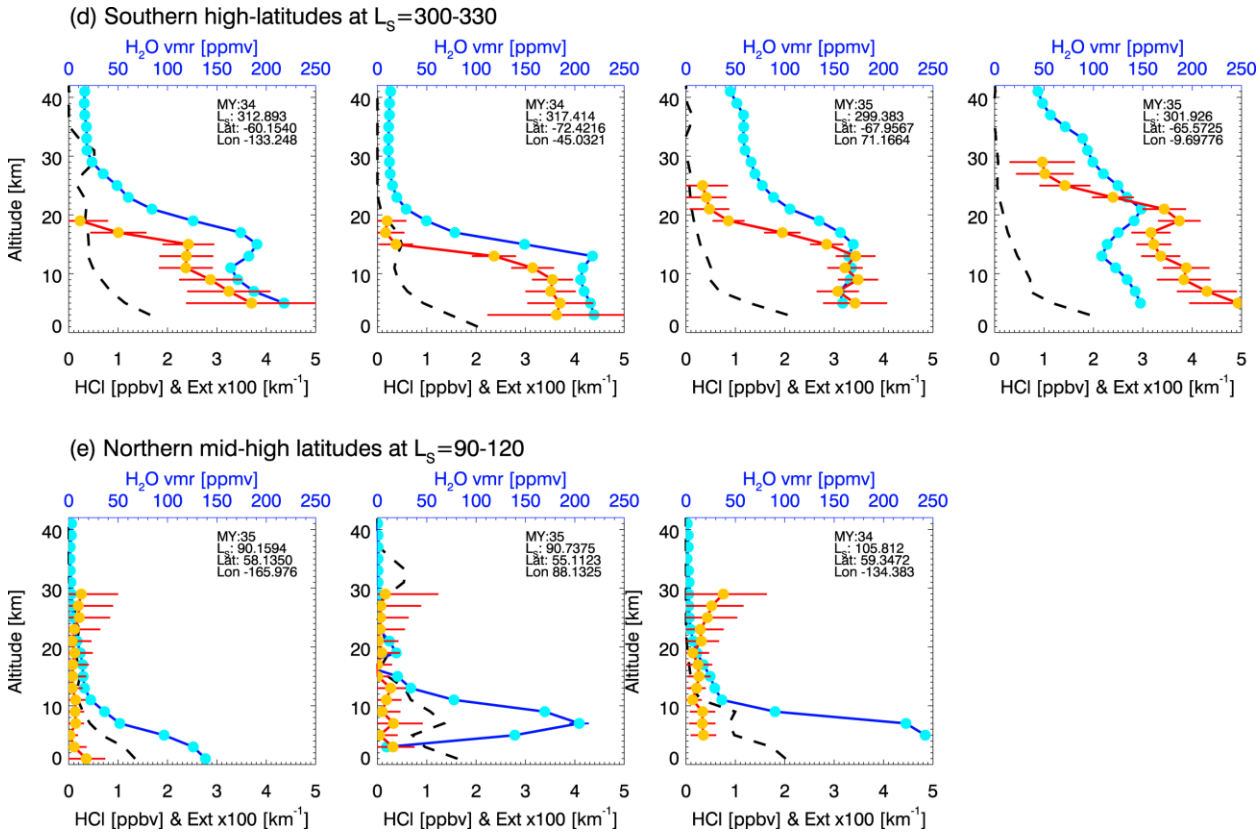

Figure 3. (Continued)

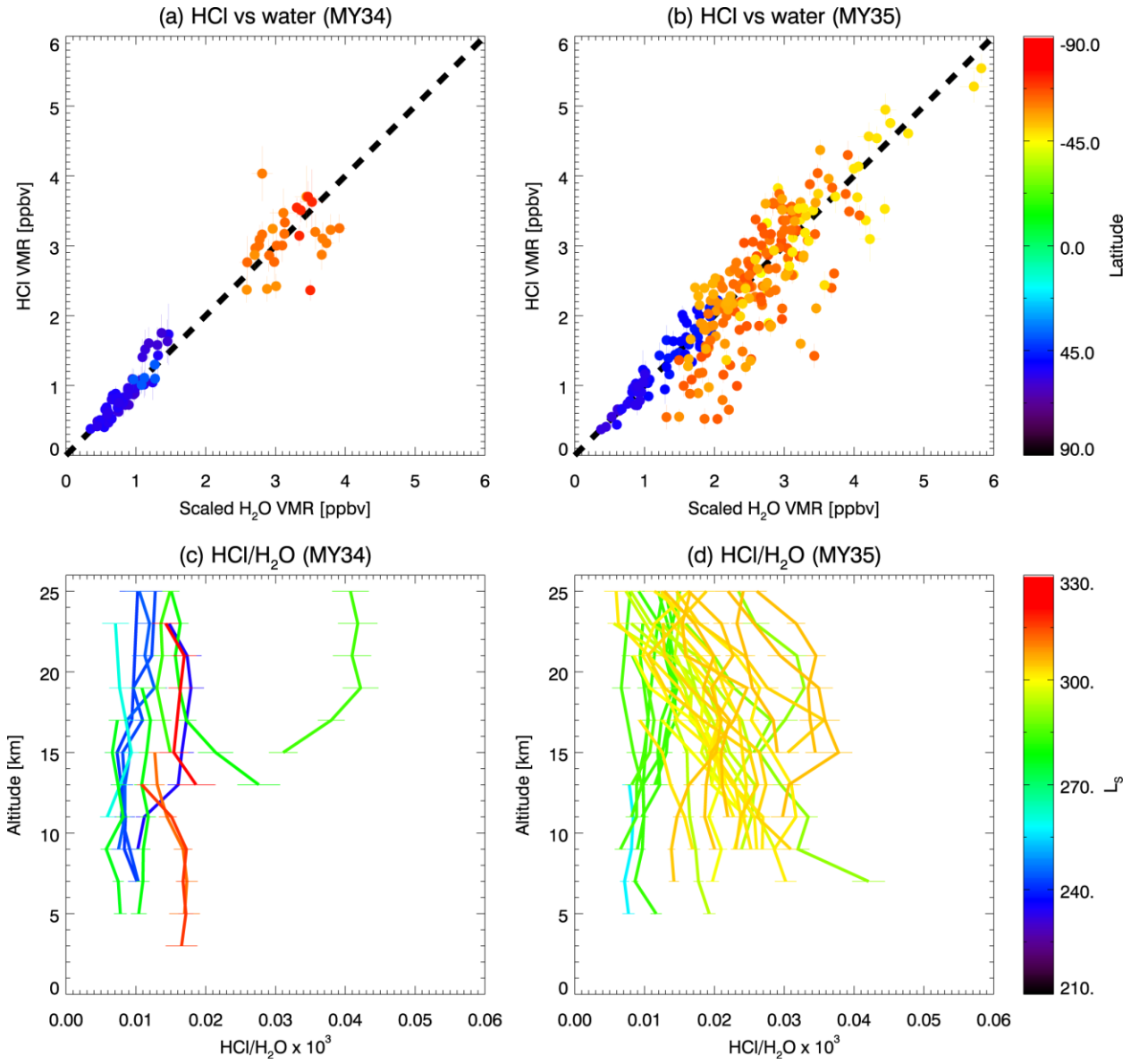

Figure 4. (a-b) HCl volume mixing ratios are plotted against scaled water vapor mixing ratios, for all profiles combined (a: MY34, b: MY35). The water vapor mixing ratios are scaled by the ratio of the HCl and H_2O partial column densities below 25 km within each profile (see SI-1). When HCl and H_2O profiles are similar in shape, their points will fall on or near the identity line. The color scale represents the latitude of the observations. (c-d) HCl/H_2O ratio for all profiles. The color scale represents solar longitude (L_s) of the observations.